vehicles

MDPI

Article

Model-Free Filter-Based Trajectory Tracking Controller for Two-Wheeled Vehicles Through Pole-Zero Cancellation Technique

Hosik Lee [1], Sangyoon Oh [2], Kyung-Soo Kim [2], Yonghun Kim [3,*] and Seok-Kyoon Kim [4,5,*]

[1] Green Mobility Team, Tenergy, Suwon 18487, Republic of Korea
[2] Department of Mechanical Engineering, Korea Advanced Institute of Science and Technology, Daejeon 34141, Republic of Korea
[3] School of Mechanical Engineering, Chungnam National University, Daejeon 136701, Republic of Korea
[4] Department of Creative Convergence Engineering, Hanbat National University, Daejeon 34158, Republic of Korea
[5] Micro Control Laboratory, Research Institute, Suwon 16521, Republic of Korea
* Correspondence: yonghun.kim@cnu.ac.kr (Y.K.); skkim77@adaptivesystem.org or lotus45kr@gmail.com (S.-K.K.)

Abstract: Considering the nonlinear dynamics, this paper devises an advanced position trajectory tracking controller with a model-free filter for two-wheeled vehicle (TWV) applications. The proposed technique preserves a simple structure in the form of the proportional–integral (PI) controller involving the model-free filter and nonlinearly structured feedback gains, which make the following contributions: (a) the proposed filter smooths the position and yaw angle measurements according to the first-order convergence rate without any model information; and (b) the PI control with the nonlinearly structured feedback gains robustly stabilizes the position and yaw angle errors along the desired first-order system to accomplish the trajectory tracking mission, which is obtained by the pole-zero cancellation (PZC) in the presence of modeling errors. MATLAB/Simulink was used to emulate the resulting feedback system and validate the effectiveness of the proposed technique.

Keywords: two-wheeled mobile robot; trajectory tracking; pole-zero cancellation

Citation: Lee, H.; Oh, S.; Kim, K.-S.; Kim, Y.; Kim, S.-K. Model-Free Filter-Based Trajectory Tracking Controller for Two-Wheeled Vehicles Through Pole-Zero Cancellation Technique. *Vehicles* **2024**, *6*, 1902–1921. https://doi.org/10.3390/vehicles6040093

Academic Editors: Yongmin Zhong and Mohammed Chadli

Received: 11 October 2024
Revised: 1 November 2024
Accepted: 5 November 2024
Published: 11 November 2024

1. Introduction

The application area of autonomous vehicles has increased dramatically to accomplish various tasks, such as military exploration, catering services, and pioneering missions. The mobile robots for these missions usually include two controllable wheels at the front and a freely moving wheel at the back, named the two-wheeled vehicle (TMV). Their movements are described by a set of fourth-order differential equations that present certain challenges, such as strong nonlinearity and under-actuation, which have attracted increasing attention from system engineers since the 1960s [1–5].

There have been numerous classical and advanced solutions for the trajectory tracking problem of TMVs through linear and nonlinear controller design approaches, which involve complicated coordinate transformations and ignore the servo motor (actuator) dynamics. It is especially unreasonable to assume that the servo motor dynamics (e.g., the transfer function) are ideal due to uncertain load variations leading to system parameter changes as well. The time-varying state-feedback controllers for the trajectory tracking problem stabilized the error dynamics by linearizing the original nonlinear system for a given operating condition [6,7]. The coordinate transformation-based nonlinear controllers alleviate the performance limitation caused by linearization and remove the dependence on operating conditions, unlike state-feedback controllers [8,9]. Another nonlinear approach depending on the coordinate transformation involves the online parameter estimators to estimate the uncertain vehicle depth and radius used for constructing the feed-forward

compensator [10]. Novel filtering techniques also enable one to handle the system parameter variation problem by continuously calculating the estimated parameters for the main controller [11–13]. Switching controls involves adaptive and back-stepping methods to solve the global tracking problem through coordinate transformations, including discontinuities [14–16]. These previous studies focused on guaranteeing global stability without demonstrating the realizations and concerning the practical challenges, such as system parameter variations, complicated coordinate transformation processes, and the idealization of actuator dynamics. The coordinate transformation-free simple ON–OFF technique addressed the concerns related to actual implementation and ensured local stability by constraining the yaw acceleration into an admissible set with the experimental validation using prototype hardware [17].

Recent results based on neural network, fuzzy, adaptive, and sliding-mode methods have improved the closed-loop performance and robustness by considering the disturbances originating from model–plant mismatches [18–23]. However, sliding-mode control involves discontinuities in both the feedback and feed-forward loops, which is a practical implementation issue. The intelligent controllers (neural network, fuzzy, and adaptive) considerably increase the computational complexity by requiring an online optimization process and numerous subsystem dynamics. The recently introduced back-stepping technique attempted to solve the discontinuity problem of sliding-mode control by including a high-performance two-time scaled disturbance observer (DOB) with rigorous stability proofs, and the performance improvements were demonstrated through a realistic numerical verification [24]. Numerical optimization-free intelligent controllers (including the DOB) automatically increase and restore the outer loop gain by the transient and steady-state operations with a stability guarantee, assuming an ideal inner loop transfer function [25,26]. This limitation can be addressed by considering uncertain servo motor dynamics, which increases the difficulty of designing the tracking controller due to the increased order of the open-loop system and a large number of sensors. The novel DOB-based results partially solved these practical problems by providing a considerably improved inner loop that exhibited a consistent performance over a wide operating region [27]. However, the absence of integral actions would limit the closed-loop robustness.

These advanced techniques involve complicated coordinate transformations and nonlinear functions for the feedback loop to ensure stability and performance, which limits the applicability for industrial applications. To address this practical challenge, the proposed solution includes a simple model-free filter for the measurements to construct an advanced proportional–integral (PI) controller ensuring the beneficial feedback system properties. The contributions of this paper are given as follows:

- The proposed model-free filter enhances the feedback loop accuracy by eliminating the reliance on the TWV model and it makes the position and yaw angle filtering error dynamics diagonal ensuring the first-order system by the nonlinear structure of the filter gain.
- The feedback signals obtained from the proposed model-free filter define the pole-zero cancellation (PZC) controller equipped with the nonlinearly structured PI gains to robustly stabilize the tracking errors satisfying the desired first-order convergence rate while attenuating the disturbances originating from the model–plant mismatches.

A feedback system analysis rigorously derives these properties, whose practical benefits were validated by conducting MATLAB/Simulink-based simulations.

2. Nonlinear Dynamics of TMV

Figure 1 represents the model of the TMVs in the Cartesian coordinate, which equips the actuators for the left- and right-side motors (generating left and right speeds ω_1 and ω_2) and one free-wheel. Since the linear combinations of actuator speed ω_1 and ω_2 determine the linear velocity v (in m/s) and yaw angular velocity ω_ϕ ($= \dot{\phi}$, in rad/s), these two variables v and ω_ϕ are treated as the input variables for changing the position $\mathbf{p} = \begin{bmatrix} x & y \end{bmatrix}^T$

acting as the output variable. Then, the system $(v, \omega_\phi) \mapsto \mathbf{p}$ can be described as the following nonlinear differential equations given by

$$\dot{\mathbf{p}} = \mathbf{f}(v, \phi, \omega_\phi, d_{cen}), \quad (1)$$
$$\dot{\phi} = \omega_\phi, \ \forall t \geq 0, \quad (2)$$

where $\mathbf{f}(v, \phi, \omega_\phi, d_{cen}) := \begin{bmatrix} v\cos(\phi) - d_{cen}\omega_\phi \sin(\phi) \\ v\sin(\phi) + d_{cen}\omega_\phi \cos(\phi) \end{bmatrix}$ with an uncertain coefficient d_{cen} representing the distance between the centers of mass and controllable wheels. The wheel radius and depth of TMVs are denoted as two uncertain coefficients R and D, respectively, which define the relationships between the velocities of v and ω_ϕ and the rotational speeds of ω_1 and ω_2 (see [28] for details).

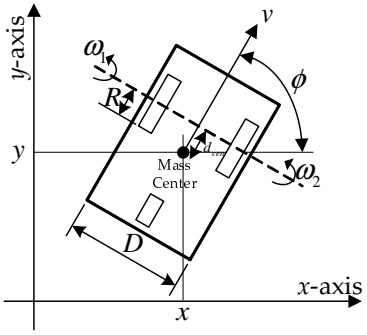

Figure 1. Model of TMVs.

3. Proposed Technique

3.1. Control Objective

This paper defines the control objective by designing reference signals v_{ref} and ϕ_{ref} for v and ω_ϕ to accomplish the exponential convergence

$$\lim_{t\to\infty} \mathbf{p} = \mathbf{p}^* \quad (3)$$

for the desired trajectory $\mathbf{p}^*$ with its tracking error $\tilde{\mathbf{p}}^* := \mathbf{p}_{ref} - \mathbf{p}^*$ satisfying

$$\dot{\tilde{\mathbf{p}}}^* = -\lambda_c \tilde{\mathbf{p}}^*, \ \forall t \geq 0, \quad (4)$$

with a given specification $\lambda_c > 0$ (convergence rate), resulting in the guarantee of the trajectory tracking mission

$$\lim_{t\to\infty} \mathbf{p} = \mathbf{p}_{ref}$$

for any given reference trajectory $\mathbf{p}_{ref}$.

3.2. Model-Free Filter

3.2.1. Position Loop

The signal decomposition $\mathbf{p} = \mathbf{p}_0 + \Delta\mathbf{p}$ for $\dot{\mathbf{p}}_0 = \mathbf{0}$ and $\Delta\dot{\mathbf{p}} \neq \mathbf{0}$, $\forall t \geq 0$, leads to the system for $\mathbf{p}_a := \begin{bmatrix} \mathbf{p} \\ \Delta\mathbf{p}_v \end{bmatrix}$ and $\Delta\mathbf{p}_v := \Delta\dot{\mathbf{p}}$:

$$\dot{\mathbf{p}}_a = \mathbf{A}_{p_a}\mathbf{p}_a + \mathbf{B}_{p_a}\mathbf{d}_{p_a}, \quad (5)$$
$$\mathbf{p} = \mathbf{C}_{p_a}^T \mathbf{p}_a, \quad (6)$$

where $\mathbf{A}_{p_a} := \begin{bmatrix} \mathbf{0}_{2\times 2} & \mathbf{I}_{2\times 2} \\ \mathbf{0}_{2\times 2} & \mathbf{0}_{2\times 2} \end{bmatrix}$, $\mathbf{B}_{p_a} := \begin{bmatrix} \mathbf{0}_{2\times 2} \\ \mathbf{I}_{2\times 2} \end{bmatrix}$, $\mathbf{C}_{p_a} := \begin{bmatrix} \mathbf{I}_{2\times 2} \\ \mathbf{0}_{2\times 2} \end{bmatrix}$, $\mathbf{d}_{p_a} := \Delta\ddot{\mathbf{p}}$, and $\|\mathbf{d}_{p_a}\| \leq \bar{d}_{p_a}$, $\forall t \geq 0$. The proposed technique filters the output $\mathbf{p}$ for the system of (5) and (6) according to the system for $\hat{\mathbf{p}}_a (= \begin{bmatrix} \hat{\mathbf{p}} \\ \Delta\hat{\mathbf{p}}_v \end{bmatrix})$ given by

$$\begin{aligned} \dot{\hat{\mathbf{p}}}_a &= \mathbf{A}_{p_a}\hat{\mathbf{p}}_a + \mathbf{L}_{p_a}(\mathbf{p} - \hat{\mathbf{p}}), & (7) \\ \hat{\mathbf{p}} &= \mathbf{C}_{p_a}^T\hat{\mathbf{p}}_a, \ \forall t \geq 0, & (8) \end{aligned}$$

equipping the nonlinearly structured filtering gain $\mathbf{L}_{p_a} = \begin{bmatrix} \mathbf{l}_{p_a,1} \\ \mathbf{l}_{p_a,2} \end{bmatrix}$ such that

$$\mathbf{l}_{p_a,1} = (k_{d,f} + \lambda_f)\mathbf{I}_{2\times 2} \text{ and } \mathbf{l}_{p_a,2} = k_{d,f}\lambda_f\mathbf{I}_{2\times 2} \quad (9)$$

by design parameters $k_{d,f} > 0$ and $\lambda_f > 0$.

3.2.2. Yaw Angle Loop

The signal decomposition $\phi = \phi_0 + \Delta\phi$ for $\dot{\phi}_0 = 0$ and $\Delta\dot{\phi} \neq 0$, $\forall t \geq 0$, leads to the system for $\boldsymbol{\phi}_a := \begin{bmatrix} \phi \\ \Delta\phi_v \end{bmatrix}$ and $\Delta\phi_v := \Delta\dot{\phi}$:

$$\begin{aligned} \dot{\boldsymbol{\phi}}_a &= \mathbf{A}_{\phi_a}\boldsymbol{\phi}_a + \mathbf{e}_2 d_{\phi_a}, & (10) \\ \phi &= \mathbf{e}_1^T\boldsymbol{\phi}_a, & (11) \end{aligned}$$

where $\mathbf{A}_{\phi_a} := \begin{bmatrix} 0 & 1 \\ 0 & 0 \end{bmatrix}$, $\mathbf{e}_1 := \begin{bmatrix} 1 \\ 0 \end{bmatrix}$, $\mathbf{e}_2 := \begin{bmatrix} 0 \\ 1 \end{bmatrix}$, $d_{\phi_a} := \Delta\ddot{\phi}$, and $|d_{\phi_a}| \leq \bar{d}_{\phi_a}$, $\forall t \geq 0$. The proposed technique filters the output ϕ for the system of (10) and (11) according to the system for $\hat{\boldsymbol{\phi}}_a (= \begin{bmatrix} \hat{\phi} \\ \Delta\hat{\phi}_v \end{bmatrix})$ given by

$$\begin{aligned} \dot{\hat{\boldsymbol{\phi}}}_a &= \mathbf{A}_{\phi_a}\hat{\boldsymbol{\phi}}_a + \mathbf{l}_{\phi_a}(\phi - \hat{\phi}), & (12) \\ \hat{\phi} &= \mathbf{e}_1^T\hat{\boldsymbol{\phi}}_a, \ \forall t \geq 0, & (13) \end{aligned}$$

equipping the nonlinearly structured filtering gain $\mathbf{l}_{\phi_a} = \begin{bmatrix} l_{\phi_a,1} \\ l_{\phi_a,2} \end{bmatrix}$ such that

$$l_{\phi_a,1} = k_{d,f} + \lambda_f \text{ and } l_{\phi_a,2} = k_{d,f}\lambda_f \quad (14)$$

by design parameters $k_{d,f} > 0$ and $\lambda_f > 0$.

Remark 1. *This remark summarizes the two major advantages of the proposed filter consisting of (7)–(9) and (12)–(14), compared with the conventional Luenberger observer-type filters (in [29,30]), such that*

- *(Model-Free)*
  The implementation of the proposed filter does not necessitate any TMV model information as it involves the known simple matrices $\boldsymbol{A}_{p_a}$, $\boldsymbol{C}_{p_a}$, $\boldsymbol{A}_{\phi_a}$, and $\boldsymbol{e}_1$, as well as the gains (9) and (14).
- *(Diagonalization for Filtering Error Dynamics)*
  The proposed model-free filter results in the diagonalized system for $\boldsymbol{e}_f := \begin{bmatrix} \boldsymbol{e}_p \\ e_\phi \end{bmatrix}$, $\boldsymbol{e}_p := \boldsymbol{p} - \hat{\boldsymbol{p}}$, and $e_\phi := \phi - \hat{\phi}$ given by

  $$\dot{\boldsymbol{e}}_f = -\lambda_f\boldsymbol{e}_f, \ \forall t \geq 0, \quad (15)$$

  by constraining the design parameter $k_{d,f}$ in a feasible region.

These two items make the performance tuning process convenient due to removal of the iterative matrix calculations for performance tuning process (e.g. finding a feasible scalar design parameter $k_{d,f} > 0$ for given $\lambda_f > 0$ in (15)). The proof of the second item is given in Section 4.

3.3. Control Law

3.3.1. Derivation of Open-Loop System

The introductions of design variables $\mathbf{u}_p = \begin{bmatrix} u_x \\ u_y \end{bmatrix}$ and $\omega_{\phi,ref}$ to the system of (1) and (2) yield

$$\dot{\mathbf{p}} = \mathbf{u}_p + \Delta\mathbf{f}(\mathbf{u}_p, v, \phi) + \bar{\mathbf{d}}_p, \ \dot{\phi} = \omega_{\phi,ref} - \tilde{\omega}_\phi, \tag{16}$$

where

$$\begin{aligned} \bar{\mathbf{d}}_p &:= d_{cen} \begin{bmatrix} -\omega_\phi \sin(\phi) \\ \omega_\phi \cos(\phi) \end{bmatrix}, \\ \Delta\mathbf{f}(\mathbf{u}_p, v, \phi) &:= -\mathbf{u}_p + \mathbf{f}(v, \phi, \omega_\phi, d_{cen}) - \bar{\mathbf{d}}_p (= \begin{bmatrix} -u_x + v\cos\phi \\ -u_y + v\sin\phi \end{bmatrix}), \ \forall t \geq 0. \end{aligned} \tag{17}$$

Then, for any given references $\mathbf{p}_{ref}$ and ϕ_{ref}, the filtered errors defined as $\tilde{\mathbf{p}} := \mathbf{p}_{ref} - \hat{\mathbf{p}}$ and $\tilde{\phi} := \phi_{ref} - \hat{\phi}$ modify system (16) as

$$\dot{\tilde{\mathbf{p}}} = -\mathbf{u}_p - \Delta\mathbf{f}(\mathbf{u}_p, v, \phi) + \mathbf{d}_p + \mathbf{C}_{f,p,1}^T \dot{\mathbf{e}}_f, \tag{18}$$

$$\dot{\tilde{\phi}} = -\omega_{\phi,ref} + \tilde{\omega}_\phi + d_\phi + \mathbf{c}_{f,\phi,1}^T \dot{\mathbf{e}}_f, \tag{19}$$

where $\mathbf{C}_{f,p,1} := \begin{bmatrix} \mathbf{I}_{2\times 2} \\ \mathbf{0}_{1\times 2} \end{bmatrix}$, $\mathbf{c}_{f,\phi,1} := \begin{bmatrix} \mathbf{0}_{2\times 1} \\ 1 \end{bmatrix}$, $\mathbf{d}_p := \dot{\mathbf{p}}_{ref} - \bar{\mathbf{d}}_p$, $d_\phi := \dot{\phi}_{ref}$, $\|\dot{\mathbf{d}}_p\| \leq \bar{d}_p$, and $|\dot{d}_\phi| \leq \bar{d}_\phi$, $\forall t \geq 0$, which are used as a basis for designing the proposed solution in Section 3.3.

Remark 2. *The nonlinear function $\Delta\boldsymbol{f}(\boldsymbol{u}_p, v, \phi)$ defined in (17) derives for reference signals v_{ref} and ϕ_{ref} that*

$$\begin{aligned} &\Delta\boldsymbol{f}(\boldsymbol{u}_p, v, \phi)\Big|_{v=v_{ref}, \phi=\phi_{ref}} = \Delta\boldsymbol{f}(\boldsymbol{u}_p, v_{ref}, \phi_{ref}) = \begin{bmatrix} -u_x + v_{ref}\cos\phi_{ref} \\ -u_y + v_{ref}\sin\phi_{ref} \end{bmatrix} = \boldsymbol{0} \\ \Leftrightarrow \ &\left[\left(v_{ref} = \sqrt{u_x^2 + u_y^2} (= \|\boldsymbol{u}_p\|) \right) \& \left(\phi_{ref} = \tan^{-1}\left(\frac{u_y}{u_x}\right) \right) \right], \ \forall t \geq 0, \end{aligned} \tag{20}$$

showing

$$\lim_{v \to v_{ref}, \phi \to \phi_{ref}} \Delta\boldsymbol{f}(\boldsymbol{u}_p, v, \phi) = \boldsymbol{0} \tag{21}$$

exponentially for any given control signal $\boldsymbol{u}_p$. This paper defines the yaw angle reference ϕ_{ref} as (20) for the following sections to ensure the property (21).

3.3.2. Yaw Angle Error Stabilization Loop

The proposed solution as an update rule for $\omega_{\phi,ref}$ stabilizes the open-loop system (19) according to the PI controller for the filtered error $\tilde{\phi} = \phi_{ref} - \hat{\phi}$ defined as

$$\omega_{\phi,ref} = k_{P,PZC}\tilde{\phi} + k_{I,PZC} \int_0^t \tilde{\phi} d\tau \tag{22}$$

equipping the nonlinearly structured feedback gains for the PZC such that

$$k_{P,PZC} = k_{d,c} + \lambda_c \text{ and } k_{I,PZC} = k_{d,c}\lambda_c \tag{23}$$

by design parameters $k_{d,c} > 0$ and $\lambda_c > 0$. Figure 2 depicts the resultant feedback system structure.

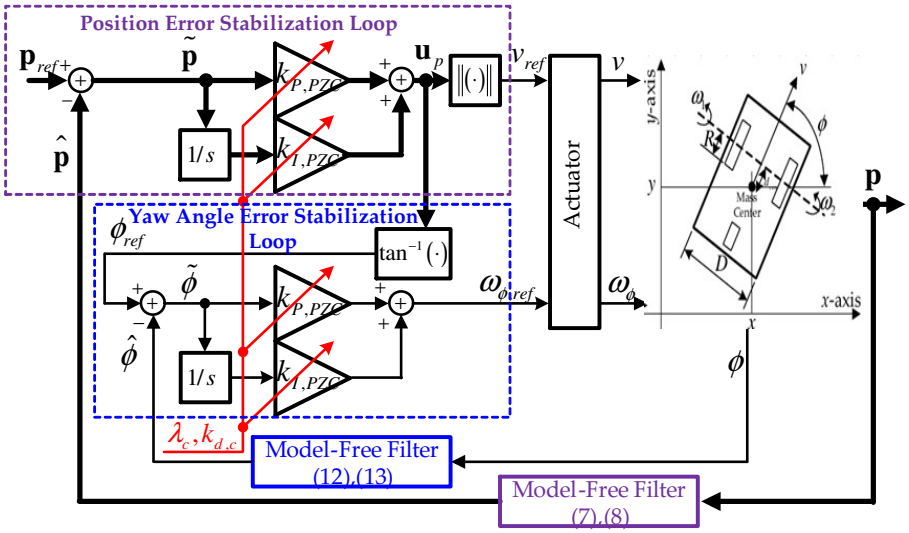

Figure 2. Proposed trajectory tracking feedback system.

The proposed solution (22) results in the controlled yaw angle error dynamics given by

$$\ddot{\tilde{\phi}} = -k_{P,PZC}\dot{\tilde{\phi}} - k_{I,PZC}\tilde{\phi} + \dot{\tilde{\omega}}_\phi + \dot{d}_\phi + \mathbf{c}_{f,\phi,1}^T \ddot{\mathbf{e}}_f, \ \forall t \geq 0, \tag{24}$$

by substituting (19) for (22), whose properties are derived in Section 4.

3.3.3. Position Error Stabilization Loop

The proposed solution as an update rule for $\mathbf{u}_p$ stabilizes the open-loop system (18) according to the PI controller for the filtered error $\tilde{\mathbf{p}} = \mathbf{p}_{ref} - \hat{\mathbf{p}}$ defined as

$$\mathbf{u}_p = k_{P,PZC}\tilde{\mathbf{p}} + k_{I,PZC}\int_0^t \tilde{\mathbf{p}} d\tau, \ \forall t \geq 0, \tag{25}$$

equipping the nonlinearly structured feedback gains for the PZC defined in (23) by design parameters $k_{d,c} > 0$ and $\lambda_c > 0$. Figure 2 depicts the resulting feedback system structure.

The proposed solution (25) results in the controlled position error dynamics given by

$$\ddot{\tilde{\mathbf{p}}} = -k_{P,PZC}\dot{\tilde{\mathbf{p}}} - k_{I,PZC}\tilde{\mathbf{p}} - \Delta\dot{\mathbf{f}}(\mathbf{u}_p, v, \phi) + \dot{\mathbf{d}}_p + \mathbf{C}_{f,p,1}^T \ddot{\mathbf{e}}_f, \ \forall t \geq 0, \tag{26}$$

by substituting (18) for (25), whose properties are derived in Section 4 considering the nonlinearly structured feedback gain of (23) designed for the PZC.

4. Feedback System Analysis Results

In this section, it is proven that the proposed trajectory tracking feedback system shown in Figure 2 guarantees the control objective (3) through further analysis for the closed-loop dynamics of (24), (26), (7)–(9), and (12)–(14). Section 4.1 starts by analyzing the model-free filter dynamics.

4.1. Model-Free Filter Analysis Results

4.1.1. Model-Free Filter for Position Loop

Lemma 1 derives the output filtering dynamics for $\mathbf{e}_p(=\ \mathbf{p}-\hat{\mathbf{p}})$ by additionally investigating the systems of (7) and (8) and its nonlinearly structured gain (9).

Lemma 1. *The model-free filter of (7) and (8) with the gain (9) forces the filtering error* $\boldsymbol{e}_p$ *to satisfy the system given by*

$$\dot{\boldsymbol{e}}_p = -\lambda_f \boldsymbol{e}_p + \boldsymbol{d}_{p_a,f} \tag{27}$$

with the excitation signal $\boldsymbol{d}_{p_a,f}$ *solving*

$$\dot{\boldsymbol{d}}_{p_a,f} = -k_{d,f}\boldsymbol{d}_{p_a,f} + \dot{\boldsymbol{d}}_{p_a},\ \forall t \geq 0. \tag{28}$$

Proof. Defining $\mathbf{e}_{p_a} := \mathbf{p}_a - \hat{\mathbf{p}}_a$, it follows from (5)–(9) that

$$\dot{\mathbf{e}}_{p_a} = \mathbf{A}_{L_{pa}}\mathbf{e}_{p_a} + \mathbf{B}_{p_a}\mathbf{d}_{p_a} \tag{29}$$

$$\mathbf{e}_p = \mathbf{C}_{p_a}^T\mathbf{e}_{p_a},\ \forall t \geq 0, \tag{30}$$

where $\mathbf{A}_{L_{pa}} := \mathbf{A}_{p_a} - \mathbf{L}_{p_a}\mathbf{C}_{p_a}^T(= \begin{bmatrix} -(k_{d,f}+\lambda_f)\mathbf{I}_{2\times 2} & \mathbf{I}_{2\times 2} \\ -k_{d,f}\lambda_f\mathbf{I}_{2\times 2} & \mathbf{0}_{2\times 2} \end{bmatrix})$, $\mathbf{B}_{p_a} = \begin{bmatrix} \mathbf{0}_{2\times 2} \\ \mathbf{I}_{2\times 2} \end{bmatrix}$, and $\mathbf{C}_{p_a} = \begin{bmatrix} \mathbf{I}_{2\times 2} \\ \mathbf{0}_{2\times 2} \end{bmatrix}$. The applications $\mathbf{E}_p(s) = \mathcal{L}\{\mathbf{e}_p\}$ and $\mathbf{D}_{p_a}(s) = \mathcal{L}\{\mathbf{d}_{p_a}\}$ to the system of (29) and (30) give

$$\mathbf{E}_p(s) = \mathbf{C}_{p_a}^T(s\mathbf{I}_{4\times 4} - \mathbf{A}_{L_{pa}})^{-1}\mathbf{B}_{p_a}\mathbf{D}_{p_a}(s),$$

where

$$\mathbf{C}_{p_a}^T(s\mathbf{I}_{4\times 4} - \mathbf{A}_{L_{pa}})^{-1}\mathbf{B}_{p_a} = \frac{1}{(s+\lambda_f)(s+k_{d,f})}\mathbf{I}_{2\times 2},\ \forall s \in \mathbb{C},$$

showing

$$(s+\lambda_f)\mathbf{E}_p(s) = \mathbf{D}_{p_a,f}(s)$$

where $\mathbf{D}_{p_a,f}(s) = (\frac{1}{s+k_{d,f}})\mathbf{D}_{p_a}(s)$, $\forall s \in \mathbb{C}$; completing the proof by $\mathbf{e}_p = \mathcal{L}^{-1}\{\mathbf{E}_p(s)\}$, $\mathbf{d}_{p_a,f} = \mathcal{L}^{-1}\{\mathbf{D}_{p_a,f}(s)\}$, and $\mathbf{d}_{p_a} = \mathcal{L}^{-1}\{\mathbf{D}_{p_a}(s)\}$. □

Lemma 2 presents the performance recovery characteristics for $\mathbf{e}_p$, eventually governed by the desired first-order dynamics subject to a feasible range for $k_{d,f} > 0$.

Lemma 2. *The model-free filter of (7) and (8) with the gain (9) ensures*

$$\lim_{t\to\infty} \boldsymbol{e}_p = \boldsymbol{e}_p^* \tag{31}$$

exponentially for the desired trajectory $\boldsymbol{e}_p^*$ *solving*

$$\dot{\boldsymbol{e}}_p^* = -\lambda_f \boldsymbol{e}_p^*,\ \forall t \geq 0, \tag{32}$$

for any $k_{d,f} > 0$ *satisfying* $\min\{\frac{2\bar{d}_{pa}}{k_{d,f}}, \frac{2\bar{d}_{\phi a}}{k_{d,f}}\} \approx 0$.

Proof. Subtracting (27) from (32) derives the system for $\boldsymbol{\epsilon}_{e_p} := \mathbf{e}_p^* - \mathbf{e}_p$ given by $\dot{\boldsymbol{\epsilon}}_{e_p} = -\lambda_f\boldsymbol{\epsilon}_{e_p} - \mathbf{d}_{p_a,f}$, which, together with (28), gives for $V_{e_p} := \frac{1}{2}\|\boldsymbol{\epsilon}_{e_p}\|^2 + \frac{\gamma_{e_p}}{2}\|\mathbf{d}_{p_a,f}\|^2$

with $\gamma_{e_p} > 0$ that $\dot{V}_{e_p} = \boldsymbol{\epsilon}_{e_p}^T(-\lambda_f \boldsymbol{\epsilon}_{e_p} - \mathbf{d}_{p_{a,f}}) - \frac{\gamma_{e_p} k_{d,f}}{2}\|\mathbf{d}_{p_{a,f}}\|^2 + \gamma_{e_p}\mathbf{d}_{p_{a,f}}^T(-\frac{k_{d,f}}{2}\mathbf{d}_{p_{a,f}} + \mathbf{d}_{p_a})$ satisfying

$$\dot{V}_{e_p} \leq -\frac{\lambda_f}{2}\|\boldsymbol{\epsilon}_{e_p}\|^2 - \frac{1}{2}(\gamma_{e_p} k_{d,f} - \frac{1}{\lambda_f})\|\mathbf{d}_{p_{a,f}}\|^2,\ \forall t \geq 0,\ \forall \|\mathbf{d}_{p_{a,f}}\| \geq \frac{2\bar{d}_{p_a}}{k_{d,f}},$$

with the application of Young's inequality, which shows

$$\dot{V}_{e_p} \leq -\alpha_{e_p} V_{e_p},\ \forall t \geq 0, \tag{33}$$

where the choices for $\gamma_{e_p} > 0$ and $k_{d,f} > 0$ as $\gamma_{e_p} = \frac{1}{k_{d,f}}(\frac{1}{\lambda_f} + 1)$ and $\min\{\frac{2\bar{d}_{p_a}}{k_{d,f}}, \frac{2\bar{d}_{\phi_a}}{k_{d,f}}\} \approx 0$ validates this inequality and $\alpha_{e_p} := \min\{\lambda_f, \frac{1}{\gamma_{e_p}}\}$; completing the proof. □

Remark 3. *The result* $\|\boldsymbol{e}_p^* - \boldsymbol{e}_p\| \approx \boldsymbol{0}$ *obtained by the result of Lemma 2 implies that* $\dot{\boldsymbol{e}}_p = -\lambda_f \boldsymbol{e}_p$ *deriving the following reasoning process with the first subsystem of (7):*

$$\begin{aligned} \ddot{\boldsymbol{e}}_p = -\lambda_f \dot{\boldsymbol{e}}_p \quad &\Leftrightarrow \quad (\Delta\dot{\boldsymbol{p}}_v - \ddot{\hat{\boldsymbol{p}}}) = -\lambda_f(\Delta\boldsymbol{p}_v - \dot{\hat{\boldsymbol{p}}}) \\ &\Leftrightarrow \quad (\Delta\dot{\boldsymbol{p}}_v - (-l_{p_a,1}\dot{\boldsymbol{e}}_p + \Delta\dot{\hat{\boldsymbol{p}}}_v)) = -\lambda_f(\Delta\boldsymbol{p}_v - (-l_{p_a,1}\boldsymbol{e}_p + \Delta\hat{\boldsymbol{p}}_v))) \\ &\Leftrightarrow \quad \dot{\boldsymbol{e}}_{\Delta p_v} - l_{p_a,1}\lambda_f \boldsymbol{e}_p = -\lambda_f \boldsymbol{e}_{\Delta p_v} - l_{p_a,1}\lambda_f \boldsymbol{e}_p \end{aligned}$$

revealing $\dot{\boldsymbol{e}}_{\Delta p_v} = -\lambda_f \boldsymbol{e}_{\Delta p_v}$ *where* $\boldsymbol{e}_{\Delta p_v} := \Delta\boldsymbol{p}_v - \Delta\hat{\boldsymbol{p}}_v$ *as the second component of* $\boldsymbol{e}_{p_a} = \boldsymbol{p}_a - \hat{\boldsymbol{p}}_a (= \begin{bmatrix} \boldsymbol{e}_p \\ \boldsymbol{e}_{\Delta p_v} \end{bmatrix} = \begin{bmatrix} \boldsymbol{p} - \hat{\boldsymbol{p}} \\ \Delta\boldsymbol{p}_v - \Delta\hat{\boldsymbol{p}}_v \end{bmatrix})$. *Therefore, this remark results in the diagonalized system given by*

$$\dot{\boldsymbol{e}}_{p_a} = -\lambda_f \boldsymbol{e}_{p_a},\ \forall t \geq 0, \tag{34}$$

concluding this subsection.

4.1.2. Model-Free Filter for Yaw Angle Loop

Lemma 3 derives the output filtering dynamics for $e_\phi (= \phi - \hat{\phi})$ by additionally investigating the system of (12) and (13) and its nonlinearly structured gain (14).

Lemma 3. *The model-free filter of (12) and (13) with the gain (14) forces the filtering error* e_ϕ *to satisfy the system given by*

$$\dot{e}_\phi = -\lambda_f e_\phi + d_{\phi_a,f} \tag{35}$$

with excitation signal $d_{\phi_a,f}$ *solving*

$$\dot{d}_{\phi_a,f} = -k_{d,f} d_{\phi_a,f} + d_{\phi_a},\ \forall t \geq 0. \tag{36}$$

Proof. Defining $\mathbf{e}_{\phi_a} := \boldsymbol{\phi}_a - \hat{\boldsymbol{\phi}}_a$, it follows from (9)–(13) that

$$\dot{\mathbf{e}}_{\phi_a} = \mathbf{A}_{l_{\phi_a}}\mathbf{e}_{\phi_a} + \mathbf{e}_2 d_{\phi_a} \tag{37}$$

$$e_\phi = \mathbf{e}_1^T \mathbf{e}_{\phi_a},\ \forall t \geq 0, \tag{38}$$

where $\mathbf{A}_{l_{\phi_a}} := \mathbf{A}_{\phi_a} - \mathbf{l}_{\phi_a}\mathbf{c}_{\phi_a}^T (= \begin{bmatrix} -(k_{d,f} + \lambda_f) & 1 \\ -k_{d,f}\lambda_f & 0 \end{bmatrix})$, $\mathbf{e}_1 = \begin{bmatrix} 1 \\ 0 \end{bmatrix}$, and $\mathbf{e}_2 = \begin{bmatrix} 0 \\ 1 \end{bmatrix}$. The applications $E_\phi(s) = \mathcal{L}\{e_\phi\}$ and $D_{\phi_a}(s) = \mathcal{L}\{d_{\phi_a}\}$ to the system of (37) and (38) give

$$E_\phi(s) = \mathbf{e}_1^T(s\mathbf{I}_{2\times 2} - \mathbf{A}_{l_{\phi_a}})^{-1}\mathbf{e}_2 D_{\phi_a}(s),$$

showing

$$\mathbf{e}_1^T(s\mathbf{I}_{2\times 2} - \mathbf{A}_{l_{\phi a}})^{-1}\mathbf{e}_2 = \frac{1}{(s+\lambda_f)(s+k_{d,f})},\ \forall s \in \mathbb{C}.$$

This implies that

$$(s+\lambda_f)E_\phi(s) = D_{\phi_a,f}(s)$$

where $D_{\phi_a,f}(s) = (\frac{1}{s+k_{d,f}})D_{\phi_a}(s)$, $\forall s \in \mathbb{C}$; completing the proof by $e_\phi = \mathcal{L}^{-1}\{E_\phi(s)\}$, $d_{\phi_a,f} = \mathcal{L}^{-1}\{D_{\phi_a,f}(s)\}$, and $d_{\phi_a} = \mathcal{L}^{-1}\{D_{\phi_a}(s)\}$. □

Lemma 4 presents the performance recovery characteristics for e_ϕ eventually governed by the desired first-order dynamics subject to a feasible range for $k_{d,f} > 0$.

Lemma 4. *The model-free filter of (12) and (13) with the gain (9) ensures*

$$\lim_{t\to\infty} e_\phi = e_\phi^* \tag{39}$$

exponentially for the desired trajectory e_ϕ^* solving

$$\dot{e}_\phi^* = -\lambda_f e_\phi^*,\ \forall t \geq 0, \tag{40}$$

for any $k_{d,f} > 0$ satisfying $\min\{\frac{2\bar{d}_{p_a}}{k_{d,f}}, \frac{2\bar{d}_{\phi_a}}{k_{d,f}}\} \approx 0$.

Proof. Subtracting (35) from (40) derives the system for $\epsilon_{e_\phi} := e_\phi^* - e_\phi$ given by $\dot{\epsilon}_{e_\phi} = -\lambda_f \epsilon_{e_\phi} - d_{\phi_a,f}$, which, together with (36), gives for $V_{e_\phi} := \frac{1}{2}\epsilon_{e_\phi}^2 + \frac{\gamma_{e_\phi}}{2}d_{\phi_a,f}^2$ with $\gamma_{e_\phi} > 0$ that $\dot{V}_{e_\phi} = \epsilon_{e_\phi}(-\lambda_f\epsilon_{e_\phi} - d_{\phi_a,f}) - \frac{\gamma_{e_\phi}k_{d,f}}{2}d_{\phi_a,f}^2 + \gamma_{e_\phi}d_{\phi_a,f}(-\frac{k_{d,f}}{2}d_{\phi_a,f} + d_{\phi_a})$ satisfying

$$\dot{V}_{e_\phi} \leq -\frac{\lambda_f}{2}\epsilon_{e_\phi}^2 - \frac{1}{2}(\gamma_{e_\phi}k_{d,f} - \frac{1}{\lambda_f})d_{\phi_a,f}^2,\ \forall t \geq 0,\ \forall |d_{\phi_a,f}| \geq \frac{2\bar{d}_{\phi_a}}{k_{d,f}},$$

with the application of the fact $\mathbf{y}^T\mathbf{z} \leq \frac{\epsilon}{2}\|\mathbf{y}\|^2 + \frac{1}{2\epsilon}\|\mathbf{z}\|^2$, $\forall \mathbf{y}, \mathbf{z} \in \mathbb{R}^n$, $\forall \epsilon > 0$ (Young's inequality), which shows

$$\dot{V}_{e_\phi} \leq -\alpha_{e_\phi}V_{e_\phi},\ \forall t \geq 0, \tag{41}$$

where the choices for $\gamma_{e_\phi} > 0$ and $k_{d,f} > 0$ as $\gamma_{e_\phi} = \frac{1}{k_{d,f}}(\frac{1}{\lambda_f} + 1)$ and $\min\{\frac{2\bar{d}_{p_a}}{k_{d,f}}, \frac{2\bar{d}_{\phi_a}}{k_{d,f}}\} \approx 0$ validates this inequality and $\alpha_{e_\phi} := \min\{\lambda_f, \frac{1}{\gamma_{e_\phi}}\}$; completing the proof. □

Remark 4. *The result $|e_\phi^* - e_\phi| \approx 0$ obtained by the result of Lemma 4 implies that $\dot{e}_\phi = -\lambda_f e_\phi$, deriving the following reasoning process with the first subsystem of (12):*

$$\begin{aligned}
\ddot{e}_\phi = -\lambda_f\dot{e}_\phi \quad &\Leftrightarrow \quad (\Delta\dot{\phi}_v - \ddot{\hat{\phi}}) = -\lambda_f(\Delta\phi_v - \dot{\hat{\phi}}) \\
&\Leftrightarrow \quad (\Delta\dot{\phi}_v - (-l_{\phi_a,1}\dot{e}_\phi + \Delta\dot{\hat{\phi}}_v)) = -\lambda_f(\Delta\phi_v - (-l_{\phi_a,1}e_\phi + \Delta\hat{\phi}_v))) \\
&\Leftrightarrow \quad \dot{e}_{\Delta\phi_v} - l_{\phi_a,1}\lambda_f e_\phi = -\lambda_f e_{\Delta\phi_v} - l_{\phi_a,1}\lambda_f e_\phi
\end{aligned}$$

revealing $\dot{e}_{\Delta\phi_v} = -\lambda_f e_{\Delta\phi_v}$ where $e_{\Delta\phi_v} := \Delta\phi_v - \Delta\hat{\phi}_v$ is the second component of $\boldsymbol{e}_{\phi_a} = \boldsymbol{\phi}_a - \hat{\boldsymbol{\phi}}_a (= \begin{bmatrix} e_\phi \\ e_{\Delta\phi_v} \end{bmatrix} = \begin{bmatrix} \phi - \hat{\phi} \\ \Delta\phi_v - \Delta\hat{\phi}_v \end{bmatrix})$. Therefore, this shows

$$\dot{\boldsymbol{e}}_{\phi_a} = -\lambda_f \boldsymbol{e}_{\phi_a},\ \forall t \geq 0, \tag{42}$$

resulting in the system for $\boldsymbol{e}_f = \begin{bmatrix} \boldsymbol{e}_p \\ e_\phi \end{bmatrix}$ *given by* $\dot{\boldsymbol{e}}_f = -\lambda_f \boldsymbol{e}_f$, $\forall t \geq 0$, *together with the result (34), which proves the statement of Remark 1.*

4.2. Control Loop Analysis Results

This section presents the control loop analysis results using the model-free filter properties provided in Section 4.1, focusing on proving the accomplishment of the control objective (3). Section 4.2.1 starts by analyzing the control loop for yaw angle error stabilization, which helps derive the main result of Section 4.

4.2.1. Control Loop for Yaw Angle Error Stabilization

Lemma 5 derives the dynamics for $\tilde{\phi}(= \phi_{ref} - \hat{\phi})$ by additionally investigating the system of (24) and its nonlinearly structured gain (23) designed for the PZC.

Lemma 5. *The proposed PI controller (22) with the gain (23) forces the error* $\tilde{\phi}$ *to satisfy the first-order system given by*

$$\dot{\tilde{\phi}} = -\lambda_c \tilde{\phi} + \tilde{\omega}_\phi + \boldsymbol{1}_3^T \boldsymbol{q}_\phi \tag{43}$$

with the excitation signal $\boldsymbol{q}_\phi (\in \mathbb{R}^3)$ *solving*

$$\dot{\boldsymbol{q}}_\phi = -k_{d,c} \boldsymbol{q}_\phi + \boldsymbol{b}_{q_\phi,1} \tilde{\omega}_\phi + \boldsymbol{B}_{q_\phi,2} \boldsymbol{e}_f + \boldsymbol{e}_3 \dot{d}_\phi, \ \forall t \geq 0, \tag{44}$$

for some $\boldsymbol{b}_{q_\phi,1} \in \mathbb{R}^3$ *and* $\boldsymbol{B}_{q_\phi,2} \in \mathbb{R}^{3\times 2}$ *where* $\boldsymbol{1}_3 := \begin{bmatrix} 1 & 1 & 1 \end{bmatrix}^T$ *and* $\boldsymbol{e}_3 := \begin{bmatrix} 0 & 0 & 1 \end{bmatrix}^T$.

Proof. The combination of (24) and the result (15) gives

$$\ddot{\tilde{\phi}} = -k_{P,PZC} \dot{\tilde{\phi}} - k_{I,PZC} \tilde{\phi} + \dot{\tilde{\omega}}_\phi + \dot{d}_\phi + \mathbf{c}_{f,\phi,2}^T \mathbf{e}_f \tag{45}$$

where $\mathbf{c}_{f,\phi,2} := \lambda_f^2 \mathbf{c}_{f,\phi,1}$, which obtains another expression for $\mathbf{x}_\phi := \begin{bmatrix} \tilde{\phi} \\ x_{\phi,2} \end{bmatrix}$ and $x_{\phi,2} := -k_{I,\phi} \int_0^t \tilde{\phi} d\tau$:

$$\dot{\mathbf{x}}_\phi = \mathbf{A}_{x_\phi} \mathbf{x}_\phi + \mathbf{b}_r r + \mathbf{e}_1 w_\phi, \tag{46}$$

$$\tilde{\phi} = \mathbf{e}_1^T \mathbf{x}_\phi, \tag{47}$$

where $\mathbf{A}_{x_\phi} := \begin{bmatrix} -(k_{d,c} + \lambda_c) & 1 \\ -k_{d,c}\lambda_c & 0 \end{bmatrix}$, $\mathbf{b}_r := \begin{bmatrix} \lambda_c \\ k_{d,c}\lambda_c \end{bmatrix}$, $\mathbf{e}_1 = \begin{bmatrix} 1 \\ 0 \end{bmatrix}$, $w_\phi := \tilde{\omega}_\phi + d_\phi + \mathbf{c}_{f,\phi,2}^T \int_0^t \mathbf{e}_f d\tau$, and dummy signal $r := 0$, $\forall t \geq 0$. The applications $\tilde{\Phi}(s) = \mathcal{L}\{\tilde{\phi}\}$, $R(s) = \mathcal{L}\{r\}$, and $W_\phi(s) = \mathcal{L}\{w_\phi\} (= \tilde{\Omega}_\phi(s) + D_\phi(s) + \frac{1}{s} \mathbf{c}_{f,\phi,2}^T \mathbf{E}_f(s))$ to the system of (46) and (47) lead to

$$\tilde{\Phi}(s) = \mathbf{e}_1^T (s\mathbf{I}_{2\times 2} - \mathbf{A}_{x_\phi})^{-1} \mathbf{b}_r R(s) + \mathbf{e}_1^T (s\mathbf{I}_{2\times 2} - \mathbf{A}_{x_\phi})^{-1} \mathbf{e}_1 W_\phi(s),$$

where the PZC by the nonlinearly structured gain (14) results in

$$\mathbf{e}_1^T (s\mathbf{I}_{2\times 2} - \mathbf{A}_{x_\phi})^{-1} \mathbf{b}_r = \frac{\lambda_c (s + k_{d,c})}{(s + \lambda_c)(s + k_{d,c})} = \left(\frac{\lambda_c}{s + \lambda_c} \right) \text{ and}$$

$$\mathbf{e}_1^T (s\mathbf{I}_{2\times 2} - \mathbf{A}_{x_\phi})^{-1} \mathbf{e}_1 = \frac{s}{(s + \lambda_c)(s + k_{d,c})}$$

showing

$$(s+\lambda_c)\tilde{\Phi}(s) = \tilde{\Omega}_\phi(s) + \sum_{i=1}^{3} Q_{\phi,i}(s)$$

where $Q_{\phi,1}(s) = -(\frac{k_{d,c}}{s+k_{d,c}})\tilde{\Omega}_\phi(s)$, $Q_{\phi,2}(s) = (\frac{1}{s+k_{d,c}})\mathbf{c}_{f,\phi,2}^T\mathbf{E}_f(s)$, and $Q_{\phi,3}(s) = (1-\frac{k_{d,c}}{s+k_{d,c}})D_\phi(s)$, $\forall s \in \mathbb{C}$; completing the proof by $\tilde{\phi} = \mathcal{L}^{-1}\{\tilde{\Phi}(s)\}$, $\tilde{\omega}_\phi = \mathcal{L}^{-1}\{\tilde{\Omega}_\phi(s)\}$, $q_{\phi,i} = \mathcal{L}^{-1}\{Q_{\phi,i}(s)\}$, $i = 1,2,3$, and $\mathbf{q}_\phi = \begin{bmatrix} q_{\phi,1} & q_{\phi,2} & q_{\phi,3} \end{bmatrix}^T$. □

Lemma 6 proves the exponential convergence for ϕ to its reference ϕ_{ref} subject to a feasible range for $k_{d,c} > 0$.

Lemma 6. *The PI controller (22) with the gain (23) ensures*

$$\lim_{t\to\infty} \phi = \phi_{ref} \tag{48}$$

exponentially for any $\phi_{ref} = \tan^{-1}(\frac{u_y}{u_x})$ *and* $k_{d,c} > 0$ *satisfying* $\min\{\frac{2\bar{d}_p}{k_{d,c}}, \frac{2\bar{d}_\phi}{k_{d,c}}\} \approx 0$, *if there exists* $\alpha_{\tilde{\omega}_\phi} > 0$ *such that*

$$\dot{\tilde{\omega}}_\phi = -\alpha_{\tilde{\omega}_\phi}\tilde{\omega}_\phi \tag{49}$$

by a well-working actuator for ω_1 *and* ω_2 *where* $\tilde{\omega}_\phi := \omega_{\phi,ref} - \omega_\phi$, $\forall t \geq 0$.

Proof. The system of (43), (44), and (49) with the result (15) gives $\dot{V}_\phi$ for $V_\phi := \frac{1}{2}\tilde{\phi}^2 + \frac{\gamma_{\phi,1}}{2}\tilde{\omega}_\phi^2 + \frac{\gamma_{\phi,2}}{2}\|\mathbf{q}_\phi\|^2 + \frac{\gamma_{\phi,3}}{2}\|\mathbf{e}_f\|^2$ with $\gamma_{\phi,i} > 0$, $i = 1,2,3$, that $\dot{V}_\phi = \tilde{\phi}(-\lambda_c\tilde{\phi} + \tilde{\omega}_\phi + \mathbf{1}_3^T\mathbf{q}_\phi) - \gamma_{\phi,1}\alpha_{\tilde{\omega}_\phi}\tilde{\omega}_\phi^2 + \gamma_{\phi,2}\mathbf{q}_\phi^T(-\frac{k_{d,c}}{2}\mathbf{q}_\phi + \mathbf{b}_{q_\phi,1}\tilde{\omega}_\phi + \mathbf{B}_{q_\phi,2}\mathbf{e}_f) - \gamma_{\phi,3}\lambda_f\|\mathbf{e}_f\|^2 + \gamma_{\phi,2}\mathbf{q}_\phi^T(-\frac{k_{d,c}}{2}\mathbf{q}_\phi + \mathbf{e}_3\dot{d}_\phi)$ satisfying

$$\begin{aligned}\dot{V}_\phi \leq\ & -\frac{\lambda_c}{3}\tilde{\phi}^2 - (\gamma_{\phi,1}\alpha_{\tilde{\omega}_\phi} - \frac{1}{4\lambda_c} - \frac{\gamma_{\phi,2}^2\|\mathbf{b}_{q_\phi,1}\|^2}{2})\tilde{\omega}_\phi^2 \\ & -(\frac{\gamma_{\phi,2}k_{d,c}}{2} - \frac{3}{4\lambda_c} - 1)\|\mathbf{q}_\phi\|^2 - (\gamma_{\phi,3}\lambda_f - \frac{\gamma_{\phi,2}^2\|\mathbf{B}_{q_\phi,2}\|^2}{2})\|\mathbf{e}_f\|^2,\end{aligned}$$

$\forall t \geq 0$, $\forall\|\mathbf{q}_\phi\| \geq \min\{\frac{2\bar{d}_\phi}{k_{d,c}}, \frac{2\bar{d}_p}{k_{d,c}}\}$ with the application of Young's inequality, which shows that

$$\dot{V}_\phi \leq -\alpha_\phi V_\phi,\ \forall t \geq 0, \tag{50}$$

where the choices for $\gamma_{\phi,i} > 0$, $i = 1,2,3$, and $k_{d,c} > 0$ as $\gamma_{\phi,1} = \frac{1}{\alpha_{\tilde{\omega}_\phi}}(\frac{1}{4\lambda_c} + \frac{\gamma_{\phi,2}^2\|\mathbf{b}_{q_\phi,1}\|^2}{2} + \frac{1}{2})$, $\gamma_{\phi,2} = \frac{2}{k_{d,c}}(\frac{3}{4\lambda_c} + \frac{3}{2})$, $\gamma_{\phi,3} = \frac{1}{\lambda_f}(\frac{\gamma_{\phi,2}^2\|\mathbf{B}_{q_\phi,2}\|^2}{2} + \frac{1}{2})$, and $\min\{\frac{2\bar{d}_\phi}{k_{d,c}}, \frac{2\bar{d}_p}{k_{d,c}}\} \approx 0$ validate this inequality and $\alpha_\phi := \min\{\frac{2\lambda_c}{3}, \frac{1}{\gamma_{\phi,1}}, \frac{1}{\gamma_{\phi,2}}, \frac{1}{\gamma_{\phi,3}}\}$; completing the proof. □

Remark 5. *By the result (48) and actuator dynamics ensuring the exponential convergence* $\lim_{t\to\infty} vs. = v_{ref}(= \|\boldsymbol{u}_p\|)$, *there exists a positive constant* $\alpha_{\Delta f}$ *such that*

$$\Delta\dot{\boldsymbol{f}}(\boldsymbol{u}_p, v, \phi) = -\alpha_{\Delta f}\Delta\boldsymbol{f}(\boldsymbol{u}_p, v, \phi),\ \forall t \geq 0, \tag{51}$$

by the fact (21) (e.g., $\lim_{t\to\infty}\Delta\boldsymbol{f}(u_p, v, \phi) = \boldsymbol{0}$ *exponentially), which is used for the remaining analysis.*

4.2.2. Control Loop for Position Error Stabilization

Lemma 7 derives the dynamics for $\tilde{\mathbf{p}}(= \mathbf{p}_{ref} - \hat{\mathbf{p}})$ by additionally investigating the system of (26) and its nonlinearly structured gain (23) designed for the PZC.

Lemma 7. *The proposed PI controller (25) with the gain (23) forces the error* $\tilde{\boldsymbol{p}}$ *to satisfy the first-order system given by*

$$\dot{\tilde{\boldsymbol{p}}} = -\lambda_c \tilde{\boldsymbol{p}} + \boldsymbol{B}_{q_p} \boldsymbol{q}_p \tag{52}$$

with the excitation signal $\boldsymbol{q}_p (\in \mathbb{R}^6)$ *solving*

$$\dot{\boldsymbol{q}}_p = -k_{d,c} \boldsymbol{q}_p + \boldsymbol{B}_{d_p,1} \Delta \boldsymbol{f} + \boldsymbol{B}_{d_p,2} \boldsymbol{e}_f + \boldsymbol{B}_{d_p,3} \dot{\boldsymbol{d}}_p, \ \forall t \geq 0, \tag{53}$$

for some $\boldsymbol{B}_{q_p} \in \mathbb{R}^{2\times 6}$, $\boldsymbol{B}_{d_p,1} \in \mathbb{R}^{6\times 2}$, *and* $\boldsymbol{B}_{d_p,2} \in \mathbb{R}^{6\times 3}$ *where* $\boldsymbol{B}_{d_p,3} := \begin{bmatrix} \boldsymbol{0}_{2\times 2} \\ \boldsymbol{0}_{2\times 2} \\ \boldsymbol{I}_{2\times 2} \end{bmatrix}$.

Proof. The combination of (26), (51), and the result (15) gives

$$\ddot{\tilde{\mathbf{p}}} = -k_{P,PZC} \dot{\tilde{\mathbf{p}}} - k_{I,PZC} \tilde{\mathbf{p}} + \alpha_{\Delta f} \Delta \mathbf{f} + \dot{\mathbf{d}}_p + \mathbf{C}_{f,p,2}^T \mathbf{e}_f \tag{54}$$

where $\mathbf{C}_{f,p,2} := \lambda_f^2 \mathbf{C}_{f,p,1}$, which obtains another expression for $\mathbf{x}_p := \begin{bmatrix} \tilde{\mathbf{p}} \\ \mathbf{x}_{p,2} \end{bmatrix}$ and $\mathbf{x}_{p,2} := -k_{I,p} \int_0^t \tilde{\mathbf{p}} d\tau$:

$$\begin{aligned} \dot{\mathbf{x}}_p &= \mathbf{A}_{x_p} \mathbf{x}_p + \mathbf{B}_r \mathbf{r} + \mathbf{B}_{x_p} \mathbf{w}_p, & (55) \\ \tilde{\mathbf{p}} &= \mathbf{C}_{x_p}^T \mathbf{x}_p, & (56) \end{aligned}$$

where $\mathbf{A}_{x_p} := \begin{bmatrix} -(k_{d,c} + \lambda_c)\mathbf{I}_{2\times 2} & \mathbf{I}_{2\times 2} \\ -k_{d,c}\lambda_c \mathbf{I}_{2\times 2} & \mathbf{0}_{2\times 2} \end{bmatrix}$, $\mathbf{B}_r := \begin{bmatrix} \lambda_c \mathbf{I}_{2\times 2} \\ k_{d,c}\lambda_c \mathbf{I}_{2\times 2} \end{bmatrix}$, $\mathbf{B}_{x_p} = \begin{bmatrix} \mathbf{I}_{2\times 2} \\ \mathbf{0}_{2\times 2} \end{bmatrix}$, $\mathbf{w}_p := \alpha_{\Delta f} \int_0^t \Delta \mathbf{f} d\tau + \mathbf{d}_p + \mathbf{C}_{f,p,2}^T \int_0^t \mathbf{e}_f d\tau$, and dummy signal $\mathbf{r} := \mathbf{0}$, $\forall t \geq 0$. The applications $\tilde{\mathbf{P}}(s) = \mathcal{L}\{\tilde{\mathbf{p}}\}$, $\mathbf{R}(s) = \mathcal{L}\{\mathbf{r}\}$, and $\mathbf{W}_p(s) = \mathcal{L}\{\mathbf{w}_p\} (= \frac{\alpha_{\Delta f}}{s} \Delta \mathbf{F}(s) + \mathbf{D}_p(s) + \frac{1}{s} \mathbf{C}_{f,p,2}^T \mathbf{E}_f(s))$ to the system of (55) and (56) lead to

$$\tilde{\mathbf{P}}(s) = \mathbf{C}_{x_p}^T (s\mathbf{I}_{4\times 4} - \mathbf{A}_{x_p})^{-1} \mathbf{B}_r \mathbf{R}(s) + \mathbf{C}_{x_p}^T (s\mathbf{I}_{4\times 4} - \mathbf{A}_{x_p})^{-1} \mathbf{B}_{x_p} \mathbf{W}_p(s),$$

where the PZC by the nonlinearly structured gain (9) results in

$$\begin{aligned} \mathbf{C}_{x_p}^T (s\mathbf{I}_{4\times 4} - \mathbf{A}_{x_p})^{-1} \mathbf{B}_r &= \frac{\lambda_c (s + k_{d,c})}{(s + \lambda_c)(s + k_{d,c})} \mathbf{I}_{2\times 2} \text{ and} \\ \mathbf{C}_{x_p}^T (s\mathbf{I}_{4\times 4} - \mathbf{A}_{x_p})^{-1} \mathbf{B}_{x_p} &= \frac{s}{(s + \lambda_c)(s + k_{d,c})} \mathbf{I}_{2\times 2} \end{aligned}$$

showing

$$(s + \lambda_c) \tilde{\mathbf{P}}(s) = \mathbf{I}_{2\times 2} \sum_{i=1}^{3} \mathbf{Q}_{p,i}(s)$$

where $\mathbf{Q}_{p,1}(s) = (\frac{1}{s + k_{d,c}}) \alpha_{\Delta f} \Delta \mathbf{F}(s)$, $\mathbf{Q}_{p,2}(s) = (\frac{1}{s + k_{d,c}}) \mathbf{C}_{f,p,2}^T \mathbf{E}_f(s)$, and $\mathbf{Q}_{p,3}(s) = (1 - \frac{k_{d,c}}{s + k_{d,c}}) \mathbf{D}_p(s)$, $\forall s \in \mathbb{C}$; completing the proof by $\tilde{\mathbf{p}} = \mathcal{L}^{-1}\{\tilde{\mathbf{P}}(s)\}$ and $\mathbf{q}_{p,i} = \mathcal{L}^{-1}\{\mathbf{Q}_{p,i}(s)\}$, $i = 1, 2, 3$, and $\mathbf{q}_p = \begin{bmatrix} \mathbf{q}_{p,1}^T & \mathbf{q}_{p,2}^T & \mathbf{q}_{p,3}^T \end{bmatrix}^T$. □

Finally, Theorem 1 proves that the proposed trajectory tracking feedback system shown in Figure 2 guarantees the establishment of the control objective (3) subject to a feasible range for $k_{d,c} > 0$ as the main result of this section.

Theorem 1. *The PI controller (25) with the gain (23) ensures that*

$$\lim_{t\to\infty} \boldsymbol{p} = \boldsymbol{p}^*$$

exponentially (e.g., establishment of the control objective (3)) for any $k_{d,c} > 0$ *satisfying* $\min\{\frac{2\bar{d}_p}{k_{d,c}}, \frac{2\bar{d}_\phi}{k_{d,c}}\} \approx 0$.

Proof. Subtracting (52) from (4) derives the system for $\boldsymbol{\epsilon}_{e_p} := \mathbf{e}_p^* - \mathbf{e}_p$ given by $\dot{\boldsymbol{\epsilon}}_{e_p} = -\lambda_c \boldsymbol{\epsilon}_{e_p} - \mathbf{B}_{q_p}\mathbf{q}_p$, which, together with (53), gives $V_p := \frac{1}{2}\|\boldsymbol{\epsilon}_{e_p}\|^2 + \frac{\gamma_{p,1}}{2}\|\mathbf{q}_p\|^2 + \frac{\gamma_{p,2}}{2}\|\Delta\mathbf{f}\|^2 + \frac{\gamma_{p,3}}{2}\|\mathbf{e}_f\|^2$ with $\gamma_{p,i} > 0$, $i = 1,2,3$, that $\dot{V}_p = \boldsymbol{\epsilon}_{e_p}^T(-\lambda_f \boldsymbol{\epsilon}_{e_p} - \mathbf{B}_{q_p}\mathbf{q}_p) + \gamma_{p,1}\mathbf{q}_p^T(-\frac{k_{d,c}}{2}\mathbf{q}_p + \mathbf{B}_{d_p,1}\Delta\mathbf{f} + \mathbf{B}_{d_p,2}\mathbf{e}_f) - \gamma_{p,2}\alpha_{\Delta f}\|\Delta\mathbf{f}\|^2 - \gamma_{p,3}\lambda_f\|\mathbf{e}_f\|^2 + \gamma_{p,1}\mathbf{q}_p^T(-\frac{k_{d,c}}{2}\mathbf{q}_p + \mathbf{B}_{d_p,3}\dot{\mathbf{d}}_{p_a})$ satisfying

$$\begin{aligned}\dot{V}_p \;\leq\; & -\frac{\lambda_f}{2}\|\boldsymbol{\epsilon}_{e_p}\|^2 - \frac{1}{2}(\gamma_{p,1}k_{d,c} - \frac{\|\mathbf{B}_{q_p}\|^2}{\lambda_f} - 2)\|\mathbf{q}_p\|^2 \\ & -(\gamma_{p,2}\alpha_{\Delta f} - \frac{\gamma_{p,1}^2\|\mathbf{B}_{d_p,1}\|^2}{2})\|\Delta\mathbf{f}\|^2 - (\gamma_{p,3}\lambda_f - \frac{\gamma_{p,1}^2\|\mathbf{B}_{d_p,2}\|^2}{2})\|\mathbf{e}_f\|^2,\end{aligned}$$

$\forall t \geq 0, \forall\|\mathbf{q}_p\| \geq \frac{2\bar{d}_{p_a}}{k_{d,c}}$, with the application of Young's inequality, concluding that

$$\dot{V}_p \leq -\alpha_p V_p,\ \forall t \geq 0,$$

where the choices for $\gamma_{p,i} > 0$, $i = 1,2,3$, and $k_{d,c} > 0$ as $\gamma_{p,1} = \frac{1}{k_{d,c}}(\frac{\|\mathbf{B}_{q_p}\|^2}{\lambda_f} + 3)$, $\gamma_{p,2} = \frac{1}{\alpha_{\Delta f}}(\frac{\gamma_{p,1}^2\|\mathbf{B}_{d_p,1}\|^2}{2} + \frac{1}{2})$, $\gamma_{p,3} = \frac{1}{\lambda_f}(\frac{\gamma_{p,1}^2\|\mathbf{B}_{p_d,2}\|^2}{2} + \frac{1}{2})$, and $\min\{\frac{2\bar{d}_\phi}{k_{d,c}}, \frac{2\bar{d}_p}{k_{d,c}}\} \approx 0$ validate this inequality and $\alpha_p := \min\{\frac{1}{\lambda_f}, \frac{1}{\gamma_{p,1}}, \frac{1}{\gamma_{p,2}}, \frac{1}{\gamma_{p,3}}\}$; completing the proof. □

Remark 6. *As pointed out in Section 3, there are four scalar design parameters, such as* $k_{d,f}$, λ_f *(for filter),* $k_{d,c}$, *and* λ_c *(for controller), which can be tuned as following iterative steps:*

- *For the model-free filter:*
  1. *Specify* $\lambda_f > 0$ *for the desired system (15) (e.g.,* $\dot{\boldsymbol{e}}_f^* = -\lambda_f \boldsymbol{e}_f^*$*).*
  2. *Adjust* $k_{d,f} > 100$ *for* $\|\boldsymbol{e}_f^* - \boldsymbol{e}_f\| \approx 0$ *through offline iterations (by Lemmas 2 and 4).*
- *For the controller:*
  1. *Specify* $\lambda_c > 0$ *for the desired system (4) (e.g.,* $\dot{\tilde{\boldsymbol{p}}}^* = -\lambda_c \tilde{\boldsymbol{p}}^*$*).*
  2. *Adjust* $k_{d,c} > 1$ *for* $\|\boldsymbol{p}^* - \boldsymbol{p}\| \approx 0$ *through offline iterations (by Lemma 6 and Theorem 1).*

This corresponds to another important result of Section 4, yielding the tuning result of the proposed technique used in Section 5.

5. Simulations

In this section, the combination of MATLAB/Simulink and C-programming implemented the proposed feedback system shown in Figure 2 to demonstrate the closed-loop effectiveness obtained from the analysis results in Section 4. The nonlinear differential Equations (1) and (2) emulated the system $(v, \omega_\phi) \mapsto (x, y)$ to describe the TMV motions with its actuator dynamics of $\dot{v} = k_c(v_{ref} - v)$ and $\dot{\omega}_\phi = k_c(\omega_{\phi,ref} - \omega_\phi)$, $\forall t \geq 0$, (e.g., $\frac{V(s)}{V_{ref}(s)} = \frac{\Omega_\phi(s)}{\Omega_{\phi,ref}(s)} = \frac{\omega_c}{s+\omega_c}$, $\forall s \in \mathbb{C}$) with a closed-loop bandwidth ω_c (rad/s) by using the ODE solver. The S-function coded by the C programming constructed the filters and

controllers through the internal interrupt service (ISR) with 1 ms of the period. Figure 3 visualizes the feedback system implementation where $\mathbf{p}_{ref} = \begin{bmatrix} x_{ref} & y_{ref} \end{bmatrix}^T$, $\mathbf{p} = \begin{bmatrix} x & y \end{bmatrix}^T$, and $\hat{\mathbf{p}} = \begin{bmatrix} \hat{x} & \hat{y} \end{bmatrix}^T$.

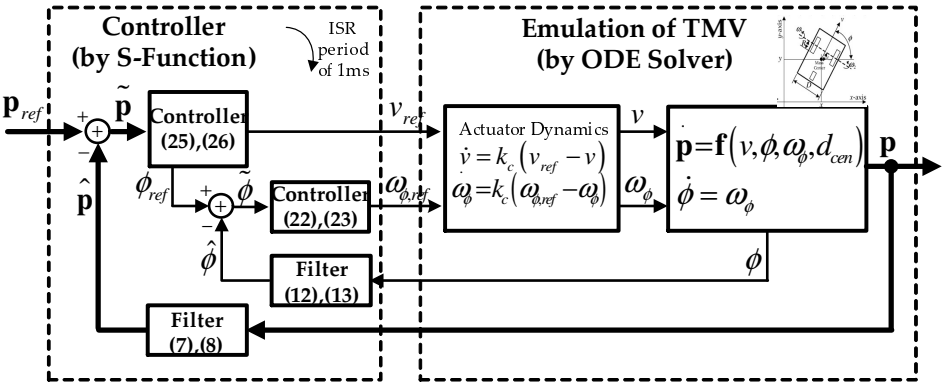

Figure 3. Feedback system implementation for simulations.

To track the reference $\mathbf{p}_{ref} = \begin{bmatrix} x_{ref} \\ y_{ref} \end{bmatrix} = \begin{bmatrix} 6\cos(2\pi f_r t) - \sin(2\pi f_r t) \\ 2\cos(2\pi f_r t) + 3\sin(2\pi f_r t) \end{bmatrix}$, $\forall t \geq 0$, with the frequency f_r Hz, representing the ellipsoidal trajectory in the Cartesian coordinate, the proposed feedback system was tuned as $k_{d,f} = 1000$ and $\lambda_f = 120$ for the model-free filter gains $l_{f,1} = k_{d,f} + \lambda_f$ and $l_{f,2} = k_{d,f}\lambda_f$ and $k_{d,c} = 5$ and $\lambda_c = 12$ for the PI gains $k_{P,PZC} = k_{d,c} + \lambda_c$ and $k_{I,PZC} = k_{d,c}\lambda_c$. The conventional PID controller is defined as

$$\begin{aligned} \mathbf{u}_p &= k_P(\mathbf{p}_{ref} - \mathbf{p}) + k_I \int_0^t (\mathbf{p}_{ref} - \mathbf{p})d\tau + k_D(\dot{\mathbf{p}}_{ref} - \dot{\mathbf{p}}), \\ \omega_{\phi,ref} &= k_P(\phi_{ref} - \phi) + k_I \int_0^t (\phi_{ref} - \phi)d\tau + k_D(\dot{\phi}_{ref} - \dot{\phi}), \ \forall t \geq 0, \end{aligned}$$

and was used to conduct the comparison studies, equipped with the well-tuned feedback gains $k_P = 3.5$, $k_I = 0.5$, and $k_D = 0.5$ for the best performance subject to the reference frequency $f_r = 0.04$ Hz and TMV parameter $d_{cen} = 0$.

5.1. Trajectory Tracking Performance Evaluation Under Various Convergence Rates

This stage evaluates the trajectory tracking performance for three reference frequencies as $f_r = 0.04$, 0.08, and 0.12 Hz with setting $d_{cen} = 0$ m for the TMV. Figure 4 presents the closed-loop position motions driven by the proposed and PID controllers, highlighting the consistent performance for three different reference speeds by the proposed controller, unlike the PID controller, where the dotted line represents the reference trajectory. The enhanced feedback system structure with the removal of the differential action obtained this closed-loop performance improvement by guaranteeing the performance recovery (by Theorem 1). Figures 5 and 6 compare the x and y axis components of $\mathbf{p}$ driven by the proposed and PID controllers in which the proposed controller successfully matched the output signals x and y and their references x_{ref} and y_{ref} despite the different operating conditions by three reference frequencies $f_r = 0.04$, 0.08, and 0.12, but the PID controller failed. The corresponding linear and angular velocity responses are presented in Figures 7 and 8, which shows the stably regulated motions, compared with the PID controller. Figure 9 visualizes the filtering error dynamics for $\mathbf{e}_x = \mathbf{x} - \hat{\mathbf{x}} (= \begin{bmatrix} x - \hat{x} \\ y - \hat{y} \\ \phi - \hat{\phi} \end{bmatrix})$ exponentially stabilized by the proposed model-free filter as the subsystem to preserve the beneficial feedback system properties.

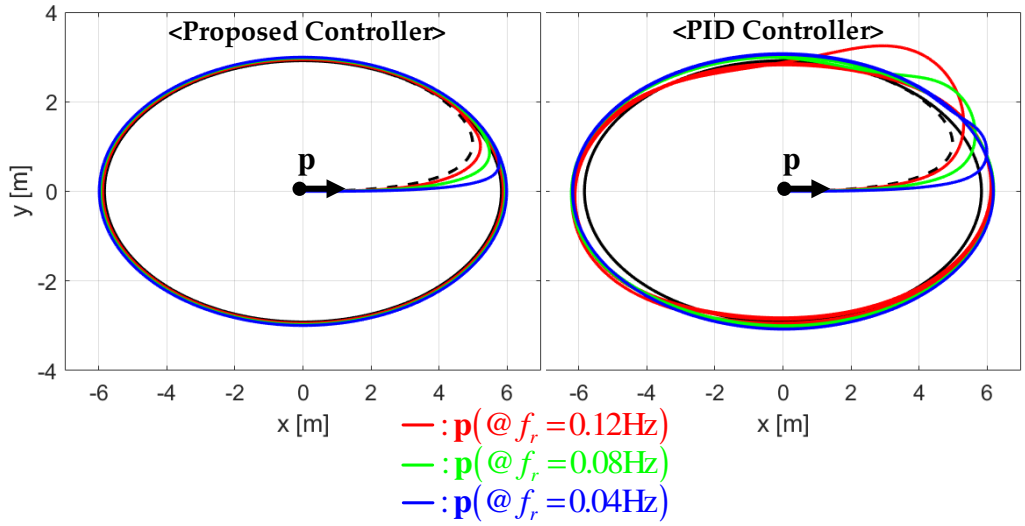

Figure 4. TMV motions in Cartesian coordinate for reference frequencies $f_r = 0.04$, 0.08, and 0.12 Hz.

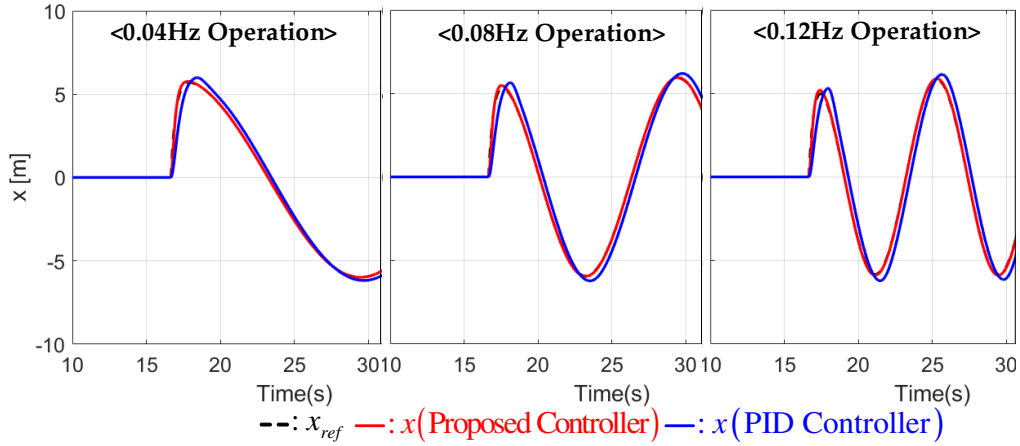

Figure 5. x axis component responses of the TMV position for reference frequencies $f_r = 0.04$, 0.08, and 0.12 Hz.

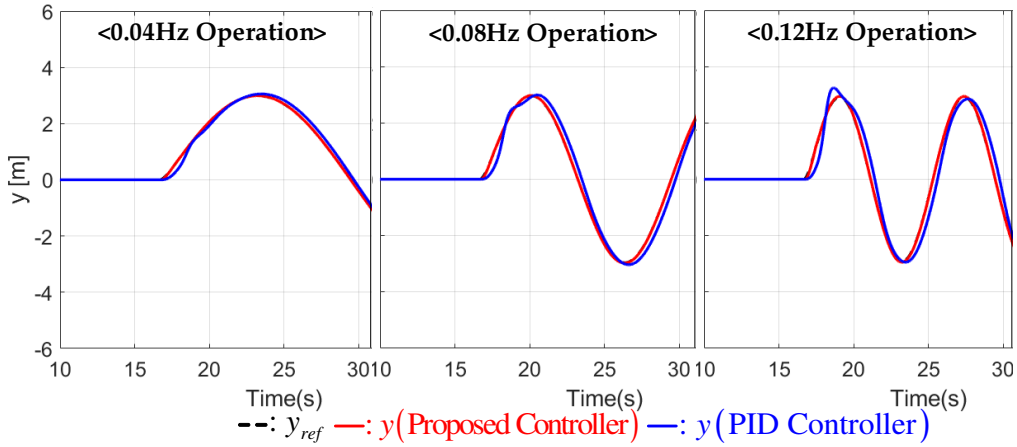

Figure 6. y axis component responses of TMV position for reference frequencies $f_r = 0.04$, 0.08, and 0.12 Hz.

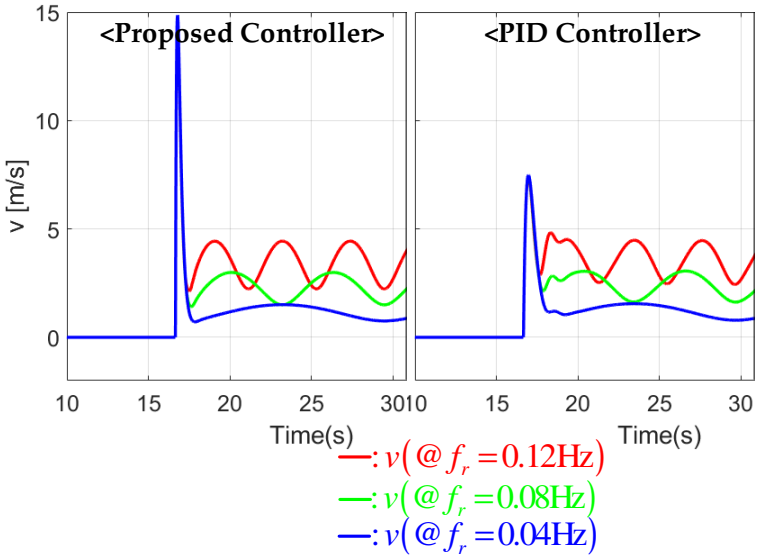

Figure 7. Linear velocity responses of TMV for the reference frequencies $f_r = 0.04$, 0.08, and 0.12 Hz.

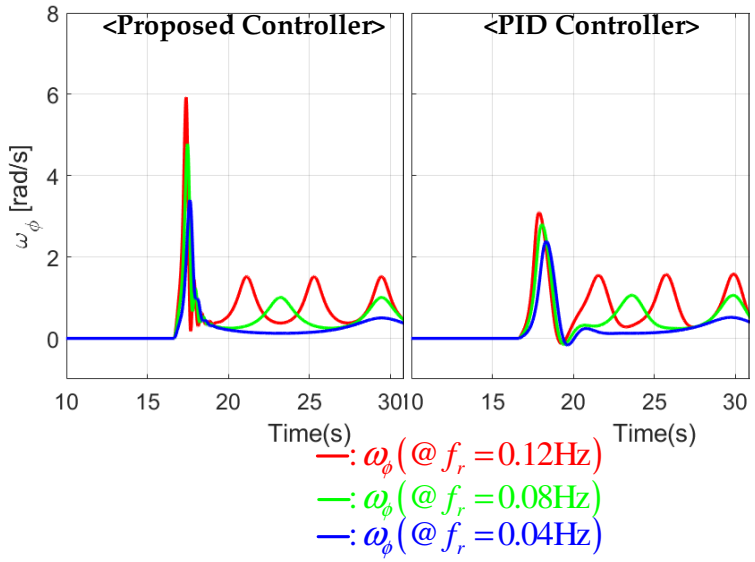

Figure 8. Yaw angular velocity responses of TMV for the reference frequencies $f_r = 0.04$, 0.08, and 0.12 Hz.

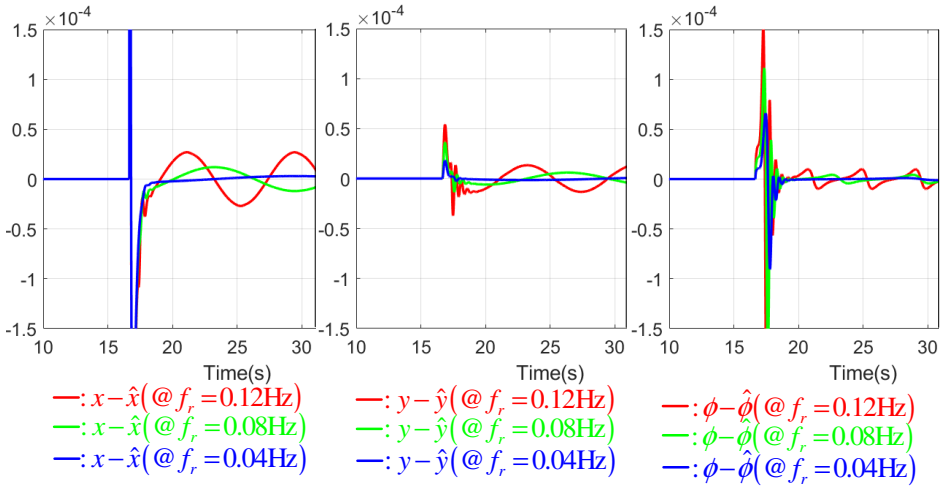

Figure 9. Filtering error responses for reference frequencies $f_r = 0.04$, 0.08, and 0.12 Hz.

5.2. Trajectory Tracking Performance Evaluation Under Various Modeling Errors

This stage demonstrates the trajectory tracking performance for three different TMV parameters of $d_{cen} = 0$, 0.3, and 0.6 m under the fixed reference frequency $f_r = 0.12$ Hz. Figure 10 implies that the proposed controller successfully rendered the TMV position dynamics consistent despite the TMV parameter variations thanks to the performance recovery proved by Theorem 1, but the PID controller failed. The corresponding x and y axis components are depicted in Figures 11 and 12, indicating their consistent behaviors by the proposed controller.

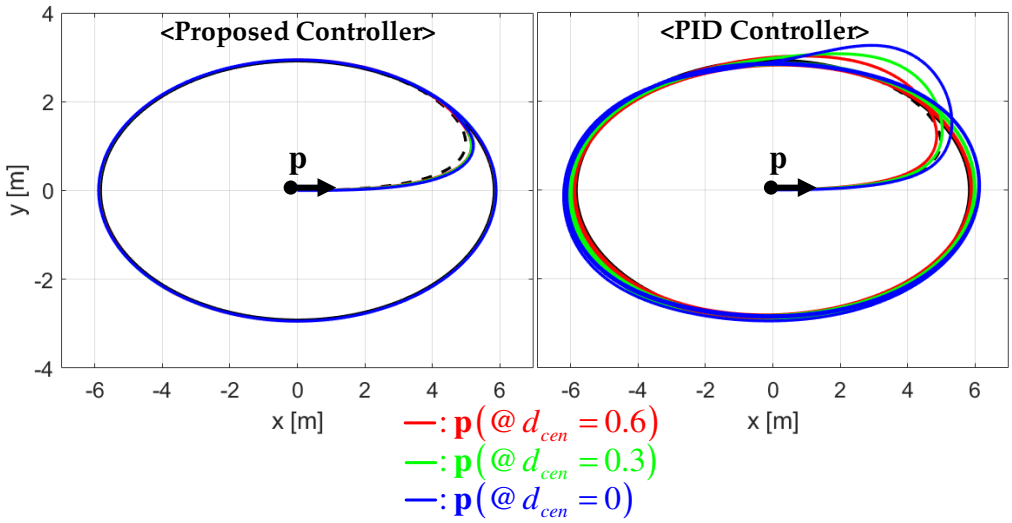

Figure 10. TMV motions in the Cartesian coordinate for different parameters $d_{cen} = 0$, 0.3, and 0.6.

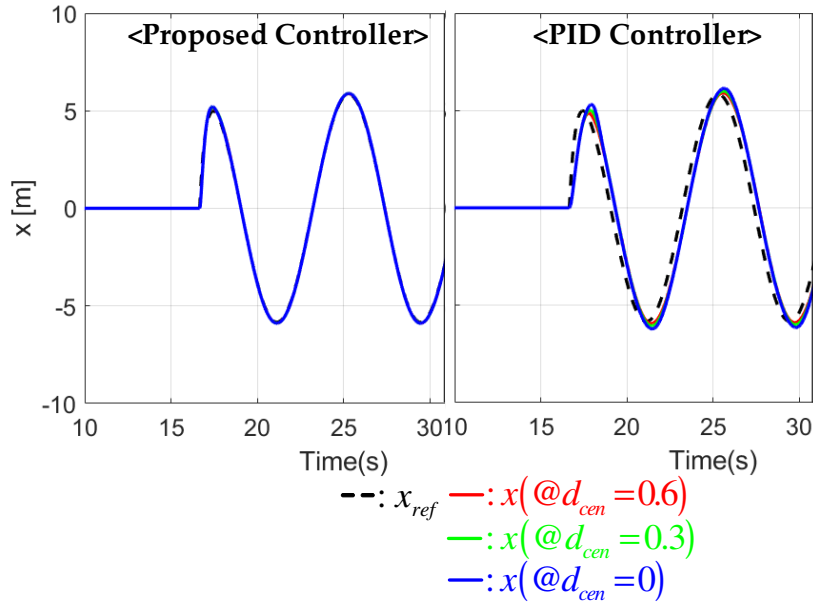

Figure 11. x axis position responses of TMV for different parameters $d_{cen} = 0$, 0.3, and 0.6.

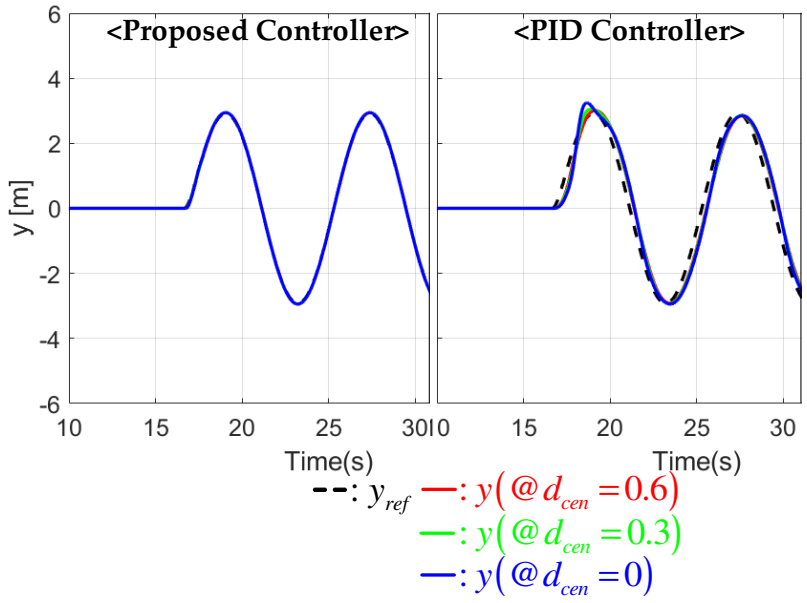

Figure 12. y axis position responses of TMV for different parameters $d_{cen} = 0$, 0.3, and 0.6.

5.3. Summary of the Tracking Performance Comparison Results

This stage ends this section by summarizing the tracking performance comparison results in Sections 5.1 and 5.2 based on the cost function for the tracking error $\mathbf{p}_{ref} - \mathbf{p}$ defined as $f_{cost} := \sqrt{\int_0^\infty \|\mathbf{p}_{ref} - \mathbf{p}\|^2 dt}$. The comparison of averaged cost values in the table of Figure 13 revealed a performance improvement of 37% by the proposed technique over the trajectory tracking scenarios in Sections 5.1 and 5.2, which will show a significant merit for the actual applications.

f_{cost}	Various Convergence Rates			Various Modeling Errors			Average
	(f_r =) 0.04Hz	0.08Hz	0.12Hz	(d_{cen} =) 0m	0.3m	0.6m	
Proposed Controller	1258	1532	1871	1875	1873	1879	1714
PID Controller	1311	1924	2723	2715	3512	4241	2737

Figure 13. Summary of tracking performance comparison results.

6. Conclusions

The proposed trajectory tracking technique was designed by forming the PI controller equipped with the nonlinearly structured feedback gains invoking the PZC, which robustly stabilizes the tracking errors, ensuring the performance recovery property despite the model–plant mismatches. The model-free filters for the imperfect position and yaw angle measurements improved the accuracy of the feedback loop to preserve this beneficial property. The realistic simulations based on MATLAB/Simulink confirmed the practical advantages of the proposed technique by demonstrating improved closed-loop performance and robustness. In future studies, the proposed technique will be applied to the industrial large-powered four-wheeled vehicles, considering the real-time constraints and actuator dynamics perturbed by the uncertain loads, with an offline optimization process yielding the best design parameters.

Author Contributions: Conceptualization and methodology, S.-K.K.; software, validation, formal analysis, investigation, writing—original draft preparation, and writing—review and editing, H.L., S.O. and Y.K.; resources, supervision, project administration, and funding acquisition, K.-S.K. and Y.K. All authors have read and agreed to the published version of the manuscript.

Funding: This work was supported by the Technology Innovation Program (20021936, Development of Verification Technology on Platform for Eco-Friendly Vehicle Tuning) funded By the Ministry of Trade, Industry & Energy (MOTIE, Korea).

Institutional Review Board Statement: Not applicable.

Informed Consent Statement: Not applicable.

Data Availability Statement: Dataset available on request from the authors.

Conflicts of Interest: The authors declare no conflicts of interest.

References

1. Lindqvist, A.L.; Zhou, S.; Halkon, B.; Aguilera, R.P.; Walker, P.D. Application of Continuous Stability Control to a Lightweight Solar-Electric Vehicle Using SMC and MPC. *Vehicles* **2024**, *6*, 874–894. [CrossRef]
2. Uchino, D.; Kobayashi, I.; Kuroda, J.; Ogawa, K.; Ikeda, K.; Kato, T.; Endo, A.; Kato, H.; Narita, T. A Basic Study for Active Steering Wheel System for Steering Burden Evaluation by Driving Position Focus on Driver's Arm Size. *Vehicles* **2023**, *5*, 846–858. [CrossRef]
3. Weinkath, M.; Nett, S.; Kim, C.D. Feasibility Study of Wheel Torque Prediction with a Recurrent Neural Network Using Vehicle Data. *Vehicles* **2023**, *5*, 605–614. [CrossRef]
4. Moreno-Gonzalez, M.; Artuñedo, A.; Villagra, J.; Join, C.; Fliess, M. Speed-Adaptive Model-Free Path-Tracking Control for Autonomous Vehicles: Analysis and Design. *Vehicles* **2023**, *5*, 698–717. [CrossRef]
5. Gao, G.; Jardin, P.; Rinderknecht, S. Linear Quadratic Tracking Control of Car-in-the-Loop Test Bench Using Model Learned via Bayesian Optimization. *Vehicles* **2024**, *6*, 1300–1317. [CrossRef]
6. Ge, S.; Wang, Z.; Lee, T. Adaptive stabilization of uncertain nonholonomic systems by state and output feedback. *Automatica* **2003**, *39*, 1451–1460. [CrossRef]
7. Marchand, N.; Alamir, M. Discontinuous exponential stabilization of chained form systems. *Automatica* **2003**, *39*, 343–348. [CrossRef]
8. Murray, R.; Sastry, S. Nonholonomic motion planning: Steering using sinusoids. *IEEE Trans. Autom. Control* **1993**, *38*, 700–716. [CrossRef]
9. Escobar, G.; Ortega, R.; Reyhanoglu, M. Regulation and tracking of the nonholonomic double integrator: A field-oriented control approach. *Automatica* **1998**, *34*, 125–131. [CrossRef]
10. Kim, M.S.; Shin, J.H.; Hong, S.G.; Lee, J.J. Designing a robust adaptive dynamic controller for nonholonomic mobile robots under modeling uncertainty and disturbances. *Mechatronics* **2003**, *13*, 507–519. [CrossRef]
11. Wang, B.; Liao, Z.; Guo, S. Adaptive Curve Passing Control in Autonomous Vehicles with Integrated Dynamics and Camera-Based Radius Estimation. *Vehicles* **2024**, *6*, 1648–1660. [CrossRef]
12. Kaliaperumal, M.; Chidambaram, R.K. Thermal Management of Lithium-Ion Battery Pack Using Equivalent Circuit Model. *Vehicles* **2024**, *6*, 1200–1215. [CrossRef]
13. Saiteja, P.; Ashok, B.; Upadhyay, D. Evaluation of Electric Vehicle Performance Characteristics for Adaptive Supervisory Self-Learning-Based SR Motor Energy Management Controller under Real-Time Driving Conditions. *Vehicles* **2024**, *6*, 509–538. [CrossRef]
14. Jiang, Z.P. Robust exponential regulation of nonholonomic systems with uncertainties. *Automatica* **2000**, *36*, 189–209. [CrossRef]
15. Tayerbi, A.; Rachid, A. Adaptive controller for nonholonomic mobile robots with matched uncertainties. *Adv. Rob.* **2000**, *14*, 105–118. [CrossRef]
16. Hespanha, J.; Liberzon, D.; Morse, A. Logic based switching control of a nonholonomic systems with parametric modeling uncertainty. *Syst. Control Lett.* **1999**, *38*, 167–177. [CrossRef]
17. Koh, K.C.; Cho, H.S. A Smooth Path Tracking Algorithm for Wheeled Mobile Robots with Dynamic Constraints. *J. Intell. Rob. Syst.* **1999**, *24*, 367–385. [CrossRef]
18. Peng, S.; Shi, W. Adaptive fuzzy integral terminal sliding mode control of a nonholonomic wheeled mobile robot. *Math. Prob. Eng.* **2017**, *2017*, 3671846. [CrossRef]
19. Ashrafiuon, H.; Nersesov, S.; Clayton, G. Trajectory tracking control of planar underactuated vehicles. *IEEE Trans. Autom. Control* **2017**, *62*, 1959–1965. [CrossRef]
20. Rossomando, F.G.; Soria, C.; Carelli, R. Neural network based compensation control of mobile robots with partially known structure. *IET Control Theory Appl.* **2012**, *6*, 1851–1860. [CrossRef]
21. Luo, S.; Wu, S.; Liu, Z.; Guan, H. Wheeled mobile robot RBFNN dynamic surface control based on disturbance observer. *ISRN Appl. Math.* **2014**, *2014*, 634936. [CrossRef]
22. Rossomando, F.G.; Soria, C.; Carelli, R. Autonomous mobile robots navigation using RBF neural compensator. *Control Eng. Pract.* **2011**, *19*, 215–222. [CrossRef]
23. Rossomando, F.G.; Soria, C.; Carelli, R. Sliding mode neuro adaptive control in trajectory tracking for mobile robots. *J. Intell. Rob. Syst.* **2014**, *74*, 931–944. [CrossRef]

24. Sun, W.; Tang, S.; Gao, H.; Zhao, J. Two time-scale tracking control of nonholonomic wheeled mobile robots. *IEEE Trans. Control Syst. Technol.* **2016**, *24*, 2059–2069. [CrossRef]
25. Kim, S.K.; Ahn, C.K. Self-Tuning Position-Tracking Controller for Two-Wheeled Mobile Balancing Robots. *IEEE Trans. Circuits Syst. II Express Briefs* **2019**, *66*, 1008–1012. [CrossRef]
26. Kim, S.K.; Ahn, C.K.; Agarwal, R.K. Position-Tracking Controller for Two-Wheeled Balancing Robot Applications Using Invariant Dynamic Surface. *IEEE Trans. Syst. Man Cybern. Syst.* **2021**, *51*, 705–711. [CrossRef]
27. Kim, S.K.; Ahn, C.K. Variable-Performance Servo System Design Without Actuator Current and Angle Measurement for Rover Vehicles. *IEEE Trans. Veh. Technol.* **2020**, *69*, 12725–12733. [CrossRef]
28. Kim, S.K.; Park, J.K.; Ahn, C.K. Learning and Adaptation-Based Position-Tracking Controller for Rover Vehicle Applications Considering Actuator Dynamics. *IEEE Trans. Ind. Electron.* **2022**, *69*, 2976–2985. [CrossRef]
29. Gao, B.; Hu, G.; Zhang, L.; Zhong, Y.; Zhu, X. Cubature Kalman filter with closed-loop covariance feedback control for integrated INS/GNSS navigation. *Chin. J. Aeronaut.* **2023**, *36*, 363–376. [CrossRef]
30. Gao, B.; Hu, G.; Zhong, Y.; Zhu, X. Cubature Kalman Filter With Both Adaptability and Robustness for Tightly-Coupled GNSS/INS Integration. *IEEE Sens. J.* **2021**, *21*, 14997–15011. [CrossRef]